

# Modular design route to construction of designer solution-processed *n*- and *p*-type nanoscale hybrid organic-inorganic thermoelectrics

Ayaskanta Sahu,<sup>1</sup> Boris Russ,<sup>1</sup> Norman Su,<sup>1,2</sup> Jason D. Forster,<sup>1</sup> Preston Zhou,<sup>1</sup> Eun Seon Cho,<sup>1</sup> Peter Ercius,<sup>3</sup> Nelson E. Coates,<sup>4</sup> Rachel A. Segalman,<sup>5</sup> and Jeffrey J. Urban<sup>1\*</sup>

<sup>1</sup>*The Molecular Foundry, Materials Sciences Division, Lawrence Berkeley National Lab, Berkeley, CA 94720, USA*

<sup>2</sup>*Department of Chemical and Biomolecular Engineering, University of California Berkeley, Berkeley, CA 94720, USA*

<sup>3</sup>*National Center for Electron Microscopy, Materials Sciences Division, Lawrence Berkeley National Lab, Berkeley, CA 94720, USA*

<sup>4</sup>*California Maritime Academy, Vallejo, CA 94720, USA*

<sup>5</sup>*Departments of Chemical Engineering and Materials, University of California Santa Barbara, Santa Barbara, CA 93106, USA*

\*email: [jjurban@lbl.gov](mailto:jjurban@lbl.gov)

## Abstract

The inability to simultaneously manipulate the thermal and electronic properties of conventional thermoelectric materials independently has impeded their progress and broad penetration into terrestrial applications. Hybrid organic/inorganic thermoelectric materials based on conducting polymers and inorganic nanostructures hold the potential to utilize both the inherently low thermal conductivity of the polymer and the superior charge transport properties of the inorganic component. While there are several successful examples of such materials, there currently exists no general design strategy for generating hybrid thermoelectric materials. Here, we combine molecular engineering at the organic/inorganic interface and simple processing techniques to demonstrate a modular approach enabling de novo design of complex hybrid thermoelectric systems. We chemically modify the surfaces of inorganic nanostructures and graft conductive polymers to yield robust solution processable *p*-type and *n*-type inorganic/organic hybrid nanostructures. We tailor the thermoelectric properties of these hybrid materials by varying the composition of the organic and inorganic components and observe novel non-monotonic behavior in the electronic properties due to strong chemical interactions between the components, which leads to peak thermoelectric performance at intermediate concentrations.

## Broader Context

Traditional composites of organic and inorganic materials demonstrate additive properties, which can be modeled by effective medium theories. However, a hybrid material offers remarkable nonlinear properties that cannot be captured by standard effective medium principles. While organic/inorganic composites have been extensively used for their improved mechanical properties, only recently have they been exploited across extremely diverse fields such as catalysis, coatings, fuel cells, optics, photovoltaics and micro-electronics. With a plethora of chemical strategies that involve integrative syntheses and innovative chemical resurfacing at the nanoscale now readily available, one can design structurally well-defined and complex hybrid nano-architectures with improved and/or unusual properties. Unfortunately, due to intrinsic chemical and morphological incongruences between hard and soft components in hybrid thermoelectric materials, it has proven extremely challenging to exert simultaneous and effective control over both charge and heat transport. We demonstrate, for the first time, a streamlined synthetic approach that allows integration of complementary functionalities in a wide-gamut of inorganic-organic hybrid systems designed specifically for thermoelectric applications. Notably, across several materials combinations, we observe electronic properties in these hybrid systems that strongly deviate from those of the individual components – owing to new transport physics that emerges from strong interactions manifest at the nanoscale interfaces between the parent constituent materials. These results highlight the importance of controlling and manipulating the surfaces of hybrid nanostructures as a simple and general but highly effective strategy to achieve macroscopic control over their thermoelectric transport properties.

## Introduction

Considering the annual increases in world-wide energy demand and thermal management needs, thermoelectric (TE) devices, which can directly interconvert thermal energy and electrical energy, and operate without any moving parts and bulk fluids, are promising technological options for power generation, waste heat recovery, and solid-state cooling.<sup>1, 2</sup> The energy conversion efficiency of a thermoelectric material is quantified by a dimensionless figure-of-merit,  $ZT = S^2\sigma T/\kappa$ , where  $S$  is the Seebeck coefficient,  $\sigma$  the electrical conductivity,  $\kappa$  the thermal conductivity ( $\kappa = \kappa_e + \kappa_l$ ) with  $\kappa_e$  and  $\kappa_l$  the electronic and lattice contributions respectively, and  $T$  the absolute temperature ( $S^2\sigma$  is typically termed as the power factor). Due to the inherently competing and conflicting nature of the parameters ( $S$ ,  $\sigma$ ,  $\kappa_e$ ) contributing to  $ZT$ , designing high  $ZT$  materials has proven challenging.<sup>3-8</sup> The first renaissance in thermoelectrics emerged when it was realized that materials with reduced dimensionalities can demonstrate higher figures of merit than their bulk counterparts due to reductions in  $\kappa_l$ , which led to a huge boom in nanostructured TEs.<sup>9-18</sup> However, the deployment of these nanostructured materials has been broadly impeded by the consumptive synthetic requirements of energy-intensive, high-temperature processing methods like molecular-beam-epitaxy, metal organic-chemical-vapor-

deposition and vapor–liquid solid approaches. Therefore, the economic viability of implementing a nanomaterial-based TE technology on a large scale using such approaches remains uncertain.

In this regard, organic materials such as polymers stand out as an attractive proposition for high performance TEs because of their inherently low thermal conductivities (1-3 orders of magnitude lower than prototypical inorganics).<sup>19</sup> Unfortunately, organics typically suffer from extremely low power factors and stability issues, which has limited their implementation as TEs. While evaporated organic thin films demonstrate high thermopowers, they are limited by poor charge carrier concentrations and/or mobilities.<sup>20</sup> In contrast, solution processed polymers<sup>21, 22</sup> and all-organic composites<sup>23</sup> with high electrical conductivities are plagued by extremely low thermopowers. Finally, an essential feature for a functional TE device is the requirement of complementary *p*- and *n*-legs, which is challenging for organic materials, as there exist very few *n*-type solution-processed organic materials that are both stable and demonstrate high TE performance.<sup>24</sup> Thus, there is an urgent need to discover novel mechanisms and classes of materials to improve *ZT*. These trends have spurred research into an entirely new class of TE materials comprising of a mixture of conductive polymers and inorganic nanostructures.

Hybrid materials are an emerging class of compounds that combine classical inorganic and organic components, where at least one of the components has dimensions ranging from a few angstroms to several nanometers, to yield materials that manifest new functionalities unattainable in traditional composites, which have additive function only.<sup>25</sup> True hybrid materials exhibit superior performance primarily due to intense non-linear interactions stemming from electronic or structural changes emerging from the nanoscale interfaces between its constituent components. Thus, hybrids comprised of inorganic nanostructures in a matrix of conducting polymer can potentially conjoin the beneficial attributes both of polymers (e.g. low thermal conductivity, solution processability, flexibility, large area and roll-to-roll production<sup>26</sup>) and inorganic nanostructures (e.g. excellent power factors, well-understood thermoelectric properties, exquisite control over size, shape and composition) to yield powerful new classes of thermoelectric materials.<sup>27</sup> While analogous hybrid materials have revolutionized the fields of photovoltaics, photodetectors, separation devices, coatings, fuel cells, catalysts,<sup>25, 28</sup> they have been surprisingly scarcely used for thermoelectric applications, primarily due to the unavailability of robust, high-performance materials. Principally, this has been due to basic chemical incompatibilities of the hard and soft components comprising hybrid thermoelectrics; this inevitably leads to electronic and morphological mismatches which commonly decimates transport. In this article, we discuss a general strategy to develop solution processed hybrid materials that implements a synergistic electronic interaction between the inorganic and organic components by re-engineering their interfacial structure and thus significantly promoting their overall thermoelectric performance. We demonstrate an unprecedented approach inspired from “*click chemistry*”<sup>29</sup> to create a myriad of thermoelectric materials comprising of a conductive polymer and a range of morphologically different inorganic components spanning from nanodots to nanoplatelets to nanowires. Not only does this strategy allow us to tap into anisotropic transport regimes but also extract fundamentally novel transport behavior since quantum confinement effects demonstrated by a zero dimensional nanocrystalline material can be radically different from a one- and a two-dimensional

semiconductor. Additionally, judicious tuning of the electronic nature of the components allows us to obtain both *n*-type and *p*-type hybrids. Finally, by varying the loading of the constituents, regardless of the identity of the components, we observe interesting non-monotonic electronic effects at intermediate loadings suggesting non-effective medium behavior which manifests from very general physics and hence presents a universal approach for obtaining high performance electronic materials.

## Results and Discussion

While the respective fields of inorganic nanostructures and conductive polymers have existed for decades, the study of hybrid materials for thermoelectrics is still in its infancy. The essential criteria for construction of thermoelectric hybrid materials are: 1) chemical compatibility of both organic and inorganic components, 2) energetic and electronic matching between both components, and 3) intimate contact spatially between components. These rigid criteria have, unfortunately, led to limited success stories of hybrid organic/inorganic materials that can potentially combine the best attributes each of these materials classes offers.<sup>30-35</sup> All hybrid materials possess the potential for property tuning simply by varying the respective composition of the component materials. However, more often than not, physical mixtures of hard and soft materials achieved by conventional blending approaches lead to uncontrolled phase segregation which not only limits the stable composition range, but also invites substantial sample to sample variation and, consequently, poor, highly erratic, and irreproducible properties.

One promising strategy is that of *in-situ* hybrid material construction, which bypasses traditional problems associated with insulating ligands used for colloidal inorganic nanostructure synthesis. In one of the first examples of this approach, See *et al.* proposed an *in-situ* synthesis that generated tellurium-PEDOT:PSS (poly(3,4-ethylenedioxythiophene) polystyrene sulfonate) nanocomposites with extremely promising thermoelectric properties ( $ZT=0.1$  at 300 K).<sup>31</sup> Interestingly, the composite material demonstrated a conductivity that was significantly higher than either component, thus characteristic of a hybrid material. This enhancement in conductivity could be attributed to a highly conductive PEDOT:PSS layer at the interface of the tellurium nanowires.<sup>33, 36, 37</sup> With a huge surface area to volume ratio, most nanostructures are susceptible to oxidation and/or chemical reactions at the interface. The PEDOT:PSS layer not only protects the tellurium (Te) nanowire from oxidation but also improves inter-particle contact so that charges can easily and efficiently flow across the device – a key requirement for a thermoelectric device.

While the *in-situ* synthetic scheme provides a general framework for us to develop the next generation of hybrid organic inorganic materials, it imposes strict restrictions owing to limited thermal stability of polymers (roughly below 150 °C). Unfortunately, temperatures required for synthesis of most inorganic nanostructures are typically in the range of 200-300 °C unlike Te (~90 °C) which severely limits the chemical tunability offered by *in-situ*

syntheses of hybrid nanostructures. Syntheses at lower temperatures often lead to amorphous nanostructures which severely impairs their charge transport properties. To alleviate the aforementioned issues, we propose an elegant synthetic approach that comprises of using the extremely well controlled syntheses of inorganic nanostructures, replacing the existing ligands (if any) with bi-functional atomic/molecular moieties which can then couple with the conductive polymer to generate the hybrid. We observe that these “click chemistry” and/or “coordination chemistry” approaches of using a linker atom or surface modification to graft conductive polymers onto or even grow the polymer of the inorganic nanoparticle surface have been extensively used in the fields of photovoltaics<sup>38</sup> and optoelectronics.<sup>39</sup> To the best of our knowledge, we demonstrate, for the first time, use of this approach to generate hybrid materials that are amenable for thermoelectric applications. Choice of the ligand or bridging moiety relies on its ability to prevent individual nanostructures from aggregation, facilitate dispersion in various solvents and facilitate linkage to a polymer of choice. In our case, we choose an extremely simple linker – sulfur atoms - which can potentially bind to any chalcogenide-based nanostructure system as well as to sulfur atoms in PEDOT (scheme portrayed in Figure 1).

Starting with syntheses of a variety of Te nanowires (with or without ligands),<sup>40-42</sup> we proceed to either replace the original ligands with sulfur ions ( $S^{2-}$ ) or functionalize the bare nanostructure surface with these  $S^{2-}$  ions (Elemental Analysis with Energy Dispersive Spectroscopy, Fig. S1, ESI†). Since the sulfur ions attached on the surface of the wires have a surface charge, they render the Te nanostructures stable in polar solvents, such as water, and prevent aggregation by electrostatic repulsion between individual nanoparticles (Zeta potential measurements, Fig. S2, ESI†). This allows us to now blend these  $S^{2-}$  capped Te nanowires with PEDOT:PSS in water. Figure 1a depicts as-synthesized bare Te nanowires without any capping ligands. Figure 1b shows the same wires with a coating of PEDOT:PSS. The approach is general and can very well be extended to other nanostructures as well. To demonstrate the versatility of our technique, we synthesize hybrid composites comprising of PEDOT:PSS and a host of different inorganic materials of various shapes and sizes varying from flat two-dimensional  $Bi_2S_3$  nanoplatelets to one-dimensional Te nanowires and spherical zero-dimensional CdSe nanocrystals (Figures 1a-f).

XRD patterns (Figure 2) show that the crystalline structure of the original nanostructure is preserved both during the surface coating with the linker as well as the coating with PEDOT:PSS. High resolution TEM images (Fig. S3, ESI†) show that while *in-situ* low temperature syntheses of Te-PEDOT:PSS yield polycrystalline samples at times,<sup>31</sup> our approach results in extremely high quality nanostructures. The amount of polymer in the hybrid can be quantified through thermogravimetric analyses (Fig. S4, ESI†). Depending on the size of the inorganic nanostructure and the thickness of the polymer coating, the weight fraction of PEDOT:PSS varies from 15% (nanoplatelets) to as low as 6% (thick nanowires). Regardless of the quantity of polymer, the resulting hybrids are highly solution-processable and can be very well dispersed in polar solvents like water (Fig. S5, ESI†) which renders them highly attractive for cheap roll-to-roll fabrication. Using drop casting followed by mild annealing ( $\sim 70$  °C) to drive off excess water, we can generate extremely smooth thin films (Fig. S6, ESI†) which show excellent thermoelectric

properties. In order to compare the performance of our hybrid materials to those generated by See and Coates *et al.* (using one-pot syntheses),<sup>31, 33</sup> we synthesize Te nanowires with almost similar diameters and aspect ratios ( $\sim 20$ ) and coat them with PEDOT:PSS. By combining additional amounts of PEDOT:PSS to the hybrids, we generate a controlled series of composites with varying organic to inorganic fraction. Figures 3a-c demonstrate the thermoelectric properties of these films while Figures 3d-f show representative composite films with different polymer to nanostructure amounts. While there are minor variations in the absolute values of the Seebeck coefficients and electrical conductivity, we are able to reproduce the same trends as was observed by Coates *et al.*, in particular the peak in electrical conductivity which was attributed to a highly conductive layer at the organic/inorganic interface (i.e. PEDOT:PSS/Te).<sup>33</sup> In spite of using an entirely different scheme to synthesize the hybrid material, we are able to obtain the same result, which highlights the powerful generality of this hybrid materials approach. Interestingly, we can now extend our approach to a wholly new material system *i.e.* bismuth sulfide nanoplatelets (Fig. S7, ESI†) coated with PEDOT:PSS and remarkably, we observe exactly similar behavior with a peak in conductivity at intermediate polymer loadings (albeit at a different concentration as compared to the Te – PEDOT:PSS system) which confirms the universality of this method. Further, the potency of this method is immediately apparent as this is the first report of using a polymeric interface to boost the thermoelectric power factor of bismuth sulfide.

Manipulating aspect ratio of nanostructures provides yet another avenue to control thermoelectric transport by opening up high electrical conductivity pathways while impairing thermal conductivity. *In-situ* techniques used for synthesis of organic-inorganic hybrids are typically system-specific and offer little control over the aspect ratio of the final product. Changing the initial polymer to inorganic precursor ratio drastically affects the nucleation and growth dynamics of the nanostructure; thus proving extremely hard to manipulate the quality, size and shape of the resulting hybrid. In contrast, our approach isolates the synthesis of the individual components from their ultimate assembly thus allowing us to exercise superior control over the morphology of the final structure. In order to demonstrate the utility of this approach, we synthesize extremely long Te-PEDOT:PSS nanowires (aspect ratios  $\sim 1000$ ) having similar diameters to those shown in Figure 3, coat them with PEDOT:PSS, repeat the casting procedure and the thermoelectric measurements (Figure 4) and compare both sets of results. We observe a five-fold increase in the maximum power factor in these long nanowires primarily due to increased electrical conductivity, which could be attributed due to lower carrier scattering from the organic/inorganic interface. One could reimagine the hybrid film to be a continuous network of percolated nanoscale interfaces. A longer nanowire leads to less number of interfaces over a certain fixed volume thus leading to a higher electrical conductivity. However, since the electronic properties are dictated by the highly conductive interfacial polymer layer, having a well-structured and smooth surface in our *ex-situ* grown NWs plays a more significant role in the improved thermopower and conductivity values. The higher quality of the interface between Te and PEDOT:PSS is very well reflected through time-resolved THz transmission measurements where we observe extremely long photoconductivity radiative lifetimes ( $\sim 40\times$  higher values) in our hybrid NWs as compared to the *in-situ* grown NWs.<sup>37</sup> These results prove that the sulfur functionalization coupled

with the PEDOT:PSS attachment results in effective passivation of the Te interface with an extremely low density of surface recombination centers and trap states.

While we have presented only one aspect of the hybrid material by tailoring the length of the nanowire, our technique presents the potential to not only optimize the size, shape and identity of the inorganic nanostructure but also the nature of the organic component. We explore this avenue by doping PEDOT:PSS with formic acid and observe a large increase in conductivity values (Fig. S8, ESI†) primarily due to the removal of insulating PSS. However, the Seebeck coefficient decreases at a much faster rate than the increase in electrical conductivity leading to a maximum power factor value similar to those obtained in Figure 4 which leads us to believe that there exists a huge scope for optimization to yield even better performances by manipulating all the above mentioned parameters.

The mechanism behind the peak in conductivity at intermediate polymer loadings was explained by Coates *et al.* with a model that invoked interfacial interactions between the inorganic nanowire and PEDOT:PSS which might lead to conformational changes in the polymer layer.<sup>33</sup> In order to control this phenomenon and enhance its beneficial effects, we need to gain a fundamental understanding about the interface. We perform X-ray photoelectron spectroscopy (XPS) studies to gain insight regarding the nature of the interaction between the inorganic and the organic components— if it is strictly a structural effect or if there is any chemical bonding/interaction between the species. XPS signals at S(2p) core edge for PEDOT:PSS (Fig. S9, ESI†) shows two distinct peaks centered around 164.5 eV and 169 eV which can be attributed to signals obtained from PEDOT and PSS respectively. In contrast, the corresponding spectra for Te-PEDOT:PSS hybrid nanowires shows a slightly higher fraction (~2%) of PEDOT peak as compared to the PSS peak which is a signature of de-doping of PEDOT:PSS<sup>43</sup> and hence points towards a chemical interaction between the inorganic and organic components rather than simply a structural/physical interaction. We presume that this de-doping could be attributed to the layer of negatively charged sulfur species (linker atoms) on our tellurium nanowires which can potentially bind to the PEDOT:PSS chains and donate electrons. However, the magnitude of this effect is tiny and hard to de-convolute since both tellurium and PEDOT:PSS are *p*-type materials.

In order to investigate if there indeed exists a charge transfer between the inorganic nanomaterial and PEDOT:PSS, we proceed to synthesize *n*-type Bi<sub>2</sub>Te<sub>3</sub> nanowires and coat them with PEDOT:PSS following the linker method described previously. Figure 5a shows a representative transmission electron micrograph for the hybrid material and Figure 5b shows X-ray diffraction patterns that depict the preservation of the crystal structure and crystallinity of the nanowire before and after polymer incorporation. Interestingly, we obtain a negative Seebeck coefficient with a modest value of nearly -19.1  $\mu\text{V}/\text{K}$  for the composite (Figure 5c) which, in principle, could simply be attributed to a mixture of an *n*- and a *p*-type material with a mean intermediate Seebeck coefficient. In order to shed more light on this issue, we perform Raman spectroscopy on thin films of samples of PEDOT:PSS and Bi<sub>2</sub>Te<sub>3</sub>-PEDOT:PSS (Figure 5d). While the Raman spectrum of pristine PEDOT:PSS shows peaks characteristic of *p*-doped PEDOT:PSS films,<sup>44, 45</sup> the peaks from the spectrum for the Bi<sub>2</sub>Te<sub>3</sub>-PEDOT:PSS film are more intense and well defined. The most

intense peak from the pristine film corresponding to  $C\alpha=C\beta$  symmetric stretching is a combination of neutral ( $1440\text{ cm}^{-1}$ ) and oxidized ( $1456\text{ cm}^{-1}$ ) PEDOT chains.<sup>45-47</sup> This peak is red-shifted in the  $\text{Bi}_2\text{Te}_3$ -PEDOT:PSS films to  $1432\text{ cm}^{-1}$  and is narrower which clearly shows the de-doping of PEDOT to neutral states. For comparison, spectrum of de-doped PEDOT:PSS with hydrazine is also shown.<sup>43, 48</sup> Evolution of a new peak at  $1521\text{ cm}^{-1}$  and disappearance of the peak at  $1260\text{ cm}^{-1}$  are further indications of the presence of de-doped PEDOT:PSS thus proving that there is a charge transfer between  $\text{Bi}_2\text{Te}_3$  and PEDOT:PSS and the interaction between the inorganic nanowire and the organic polymer is undoubtedly of a chemical nature.<sup>49</sup>

As demonstrated earlier, we can generate a controlled series of  $\text{Bi}_2\text{Te}_3$ -PEDOT:PSS composites with varying polymer fractions by adding additional amounts of PEDOT:PSS to the as-synthesized hybrid. The Seebeck coefficients of the resulting series of materials are plotted in Figure S10 (ESI†) and show a gradual progress from positive to negative values with increasing  $\text{Bi}_2\text{Te}_3$  fraction (*n*-type component). These experimentally obtained values lie between the predicted boundaries as modeled by either series or parallel connected binary composite thus characteristic of a simple mixture.<sup>50</sup> However, the true hybrid nature of this system is revealed when the composite (PEDOT:PSS portion) is doped with formic acid.<sup>51</sup> The Seebeck coefficients of the resulting series display a non-monotonic behavior with values consistently higher than PEDOT:PSS over a wide range of concentrations (Figure 6a). This behavior cannot be captured by either series or parallel models and thus, cannot be explained by mean field theories. We hypothesize that while on one hand,  $\text{Bi}_2\text{Te}_3$  nanowires reduce the hole concentration in PEDOT:PSS by de-doping, thus increasing the Seebeck coefficient; the templating of the PEDOT:PSS chains by the  $\text{Bi}_2\text{Te}_3$  nanowires might lead to increased hole mobilities along the interfacial layer. This interplay between carrier concentrations and mobilities can explain the initial increase in conductivity (Figure 6b) where the increase in mobility dominates the drop in carrier concentration. At higher  $\text{Bi}_2\text{Te}_3$  concentrations, the carrier concentration is reduced enough to dominate whatever increased hole mobility might be introduced by the restructuring of the polymer around the nanowire and thus, we observe a subsequent decrease in conductivity. The maximum power factor ( $\sim 24\text{ }\mu\text{W/m.K}^2$ ) obtained from this system coincided with the concentration of wires that showed a peak in conductivity (Figures 6b and 6c). This technique thus presents an amenable way to tune the thermoelectric properties of heavily doped polymeric materials by controlled de-doping using an inorganic additive.

Ultimately, for a working thermoelectric module, one requires both high-performing and complementary *p*-type and *n*-type materials. Traditionally, it has been extremely hard to synthesize stable, solution-processable and efficient *n*-type organics which has, in turn, limited the performance and applicability of *n*-type hybrid material systems. While we were able to obtain high-performing *p*-type hybrids using the Te-PEDOT:PSS system, we wanted to demonstrate the generality and versatility of our approach and extend it to *n*-type materials as well. Unfortunately, PEDOT:PSS is a *p*-type material and even using an *n*-type inorganic material like  $\text{Bi}_2\text{Te}_3$  did not yield composite materials with high *n*-type performance. However, the observation that PEDOT:PSS can potentially be de-doped by  $\text{Bi}_2\text{Te}_3$  through electron transfer motivated us to pursue an approach where if we manage to invert the nature of the majority charge carrier (from holes to electrons) in PEDOT:PSS



and possibly take advantage of the high mobility offered by aligned PEDOT:PSS chains, we can, in principle, obtain *n*-type hybrids with promising thermoelectric properties. In order to remove all holes from PEDOT:PSS, we use an extrinsic de-doping approach wherein we soak our Bi<sub>2</sub>Te<sub>3</sub>-PEDOT:PSS films (synthesized and cast as described earlier) in various well-known reducing agents used to modulate the optical properties of PEDOT:PSS such as sodium sulfite, sodium thiosulfate, sodium hydroxide and hydrazine hydrate.<sup>48</sup> The hydrazine hydrate treated samples gave us the best performance in terms of film quality as well as thermoelectric properties. We used a 2-step process to generate our films. First, we soaked the as-cast hybrid films in formic acid (or ethylene glycol) to remove insulating PSS and yield highly ordered and conductive (*p*-type) Bi<sub>2</sub>Te<sub>3</sub>-PEDOT hybrids (please note that this treatment renders the films insoluble in solvents like water). Subsequently, these films were dipped in hydrazine monohydrate (~5 volume % in water) to reduce PEDOT for around 10 minutes and dried at ~80 °C for nearly 20 minutes to remove any residual solvents. XPS results (Fig. S11, ESI†) demonstrate only one peak at 163.5 eV and clearly show no evidence of peaks corresponding to PSS confirming the success of the two-step process to effectively de-dope PEDOT:PSS (Fig. S9, ESI†). The peak at 163.5 eV is also red shifted by nearly 1 eV from what would be expected to be obtained from PEDOT (164.5 eV). These results hint towards complete removal of insulating PSS from PEDOT:PSS as well as intense *n*-type doping of PEDOT. We performed the treatment for a range of different concentrations of Bi<sub>2</sub>Te<sub>3</sub> and PEDOT:PSS films and the thermoelectric properties are summarized in Figures 6d-f. Comparing data from Figures 6a, b and 6d, e for the sample with just PEDOT:PSS, we observe that while the Seebeck coefficient increases from ~15 μV/K to ~100 μV/K, the electrical conductivity drops from ~560 S/cm to ~0.2 S/cm which confirms effective reduction. The Seebeck coefficients for all the analyzed samples were negative within the experimental range (16-63% by volume and 58-93% by weight of Bi<sub>2</sub>Te<sub>3</sub>) thus implying that all our hybrids were *n*-type (Figure 6d). As observed in all our previous data, we note a peak in conductivity for the samples with nearly 80 % (by weight) Bi<sub>2</sub>Te<sub>3</sub> (Figure 6b) which results in a maximum power factor of ~16 μW/m.K<sup>2</sup> which is amongst the highest reported values for an *n*-type hybrid material (Figure 6c).

## Conclusions

In conclusion, we use a lego-like approach to synthesize both *p*-type and *n*-type hybrid thermoelectrics using a conductive polymer (PEDOT:PSS) and various nanostructured inorganic materials. We use an interface engineering technique to coat our nanostructures with a linker molecule that binds to the polymer as well thus generating a robust composite. Our unique approach leads to intricate control over the organic and inorganic components and provides synergistic contact at the interface which manifests in extremely promising thermoelectric properties for the hybrid material. The strategies discussed in this report could be readily extended to other polymers and organic materials rather than being limited to PEDOT:PSS and generate novel composites. With the advent of new *n*-type organic materials, the methodology could be employed to generate hybrids which are more conducive towards electron transport as compared to PEDOT:PSS. While we demonstrated potential applications for thermoelectrics, the possibility to generate both *n*- and *p*-type

hybrid materials not only holds promise for other electronic applications but also for exploring fundamental principles like carrier filtering and phonon scattering. The development of these hybrid materials not only opens up a whole realm of new opportunities for realizing low cost, flexible and high performance thermoelectrics but also complements a very fundamental area of science by providing a platform for crucial studies on interfacial electron and phonon transport dynamics.

## Experimental Section

### Chemicals and Substrates

Tellurium dioxide (99.9995%), sodium hydroxide (ACS reagent,  $\geq 97.0\%$ , pellets), potassium hydroxide ( $\geq 85\%$  KOH basis, pellets, white), polyvinylpyrrolidone (PVP, average molecular weight  $\sim 55,000$ ), ethylene glycol (ReagentPlus<sup>®</sup>,  $\geq 99\%$ ), hydrazine hydrate (78-82%, iodometric), sodium tellurite ( $-100$  mesh, 99%), bismuth (III) chloride (99.99%, trace metals basis), oleylamine (technical grade, 70%), sulfur (99.998% trace metals basis), trioctylphosphine (technical grade, 90%), cadmium oxide ( $\geq 99.99\%$  trace metals basis), hexadecylamine (technical grade, 90%), selenium pellets (99.999%), ethylene glycol (99.9%), formic acid (reagent grade,  $\geq 95\%$ ), bismuth (III) nitrate pentahydrate ( $\geq 99.99\%$  trace metals basis) and methanol (reagent grade, 98%) were purchased from Sigma Aldrich. Acetone (J.T.Baker<sup>®</sup>) and isopropyl alcohol (ACS Grade) were purchased from VWR International. Sodium sulfide (anhydrous, min. 99.5%) were purchased from Strem Chemicals. N-dodecylphosphonic acid was purchased from PCI Synthesis. Poly(3,4-ethylenedioxythiophene) polystyrene sulfonate (PEDOT:PSS, Clevis PH 1000) was purchased from Heraeus Quartz. All chemicals were used as delivered without further purification. Quartz substrates, 9.5 mm X 9.5 mm, and 0.2 mm thick, were purchased from Thin Film Devices.  $\langle 100 \rangle$ -oriented, boron-doped silicon (Si) wafers (resistivity=0.005–0.01  $\Omega\text{cm}$ , thickness=525 $\pm$ 25  $\mu\text{m}$ ) coated with 300 nm of thermal oxide ( $\text{SiO}_2$ ) were purchased from Silicon Valley Microelectronics.

### Synthesis of Hybrid Nanostructures

All inorganic nanostructures (bare tellurium nanowires,<sup>40</sup> tellurium nanowires with ligands,<sup>41, 42</sup> cadmium selenide nanocrystals,<sup>52</sup> bismuth sulfide nanoplatelets,<sup>53</sup> bismuth telluride nanowires<sup>32</sup>) were synthesized by established literature protocols. For the surface engineering with  $\text{S}^{2-}$ , a typical reaction involved adding requisite amounts of  $\text{Na}_2\text{S}$  (typically 4-5 times the number of surface atoms on the nanostructure) in water to a 4-5 mg/ml dispersion of nanostructures in water or hexane in a glass jar with continuous stirring. Stirring periods varied between 30 minutes to overnight ( $\sim 16$  hours) depending on the specific system. After the reaction was stopped, the sulfur-capped nanostructures were centrifuged for  $\sim 45$  minutes. While the nanostructures crashed out of the dispersion, any unreacted  $\text{Na}_2\text{S}$  and starting ligands (if any) stripped from the nanostructures remained in the supernatant which was discarded. The precipitated nanostructures were dispersed in

water and isolated again with centrifugation. The process was repeated at least 4 times to ensure the removal of any unbound species and obtain a clean product. Subsequently, an excess of PEDOT:PSS (typically 2-3 times the number of surface atoms on the nanostructure) was added to the nanostructures suspended in water and the mixture was stirred overnight followed by numerous (3-4) rounds of precipitation and re-dispersion until all unbound PEDOT:PSS was removed from the suspension. Finally, the PEDOT:PSS capped nanostructures were resuspended in ultrapure 18 M $\Omega$  water and stored for further use.

### **Sample Characterization**

X-ray diffraction (XRD), scanning electron microscopy (SEM), energy dispersive x-ray spectroscopy (EDS), transmission electron microscopy (TEM), thermo-gravimetric analysis (TGA), x-ray photoelectron spectroscopy (XPS), and Raman spectroscopy were used to characterize the size, shape, structure, composition, and optical properties of the nanostructures. For the XRD, XPS, Raman measurements and SEM imaging, we used quartz substrates which were sonicated in acetone, isopropanol, and methanol (10 min in each), rinsed with methanol, dried at 100 °C for nearly 15 minutes and then UV-ozone treated for 30 minutes. For wide angle XRD, a Bruker-GADDS 8 microdiffractometer was utilized to collect wide-angle powder patterns (Cu-K $\alpha$ ). Samples were prepared from concentrated dispersions of nanostructures in solution. Films of these nanostructures were deposited onto heavily doped Si wafers covered with a thermally grown 300-nm-thick SiO<sub>2</sub> layer. For TEM, a Libra120 and an FEI Technai G20 Super Twin Lab6 microscope were used to image the nanostructures with acceleration voltages of 120 and 200 kV respectively. Each sample was prepared by depositing a drop of dilute dispersion in solvents like hexane or methanol onto a 400-mesh carbon-coated copper grid and allowing the solvent to evaporate at room temperature. SEM images were recorded and EDS analyses were performed on a Zeiss Gemini Ultra-55 Analytical Scanning Electron Microscope using beam energy of 5 kV and an In-Lens detector. TGA was acquired using a Thermal Advantage Q20 calorimeter at a scan rate of 10 °C min<sup>-1</sup>. An indium standard was used to calibrate the instrument and nitrogen was used as the purge gas. X-ray Photoelectron spectra were acquired using PHI 5400 X-ray Photoelectron Spectroscopy (XPS) System with Al K $\alpha$  source. The energy resolution was set to 0.1 eV and the experimental chamber had a base pressure of 1 $\times$ 10<sup>-9</sup> torr. Spectral fitting was performed using Casa XPS analysis software. Spectral positions were corrected by shifting the primary C 1s core level position to 284.8 eV, and curves were fit with quasi-Voigt lines following Shirley background subtraction. Confocal Raman microscopy was performed using a WITec alpha300 S confocal microscope coupled to a Raman spectrometer (1800 grooves/mm grating) equipped with a CCD detector (UHTS-300). A fiber-coupled laser operating at 532 nm was used to stimulate Raman scattering. Excitation laser light was focused into the sample with a Nikon E Plan objective lens with 20 $\times$  magnification and NA = 0.4. Light from the sample was collected using the same lens and passed through a fluorescence filter to remove nonscattered and Rayleigh-scattered laser light and then focused onto a pinhole at the entrance of an optical fiber that leads to the spectrometer. Spectra were collected using 30-60 s integration time.

### **Thermoelectric Measurements**

Films of nanostructures (typically 5 microns thick) were drop-cast onto a pre-cleaned quartz substrate (as described above) from a 100 mg/ml dispersion in water and heated at 70 °C for nearly 30 minutes. For conductivity and Seebeck measurements, four 100-nm thick gold contacts were deposited near the four corners of the drop cast films via thermal evaporation. Electrical conductivity was measured using a Keithley 2400 Sourcemeter in 4-wire van-der-Pauw configuration. Film thicknesses were estimated by scratching the nanowire film and measuring the step change with a Veeco Dektak 150 profilometer. Seebeck coefficient was measured using a homemade setup consisting of two Peltier devices (Ferrotec) spaced ~4 mm apart. Current was driven through the devices in opposing polarities, resulting in a temperature gradient about room temperature which varied with the magnitude of the current. The temperature of the sample was measured using two T-type thermocouples mounted in micromanipulators. Silicon thermal paste (Wakefield Thermal S3 Solutions) was utilized between the Peltier devices and the substrate to ensure good thermal contact. Typically, 5 different temperature gradients ( $\Delta T = +15$  °C) were employed with an equilibration time of 120-180 seconds between temperature changes, and 10-20 measurements were taken for open circuit voltage ( $V_{OC}$ ) and averaged using an Agilent 34401 multimeter. Data for both electrical conductivity and thermopower were acquired using homemade Labview programs. The value of  $V_{OC}$  varied linearly with  $\Delta T$  for all of the films within the temperature range measured. Seebeck coefficients were calculated by a linear fit of  $V_{OC}$  vs  $\Delta T$ .

## Acknowledgements

We gratefully acknowledge support through the Department of Energy BES-LBL Thermoelectrics Program. This work was partially performed at the Molecular Foundry, Lawrence Berkeley National Laboratory, and was supported by the Office of Science, Office of Basic Energy Sciences, Scientific User Facilities Division, of the U. S. Department of Energy under Contract No. DE-AC02-05CH11231. B.R. and N.S gratefully acknowledge the Department of Defense, AFOSR, for fellowship support under the National Defense Science and Engineering Graduate Fellowship (DOD-NDSEG). E.S.C. acknowledges support from the Department of Energy Grant no. DE-FG07ER46426, by the Bay Area Photovoltaic Consortium (BAPVC), funded under the Sunshot Initiative of DOE.

## Figure Captions

**Scheme 1:** Inorganic nanostructure – PEDOT:PSS hybrids. The surface of the inorganic material (nanocrystals, nanoplatelets or nanowires) is functionalized with a linker molecule ( $S^{2-}$  in this case) which binds to PEDOT:PSS as well forming a bridge between the inorganic and organic components resulting in a robust inorganic-organic hybrid material.

**Figure 1.** Transmission electron microscope (TEM) images showing tellurium nanowires (a) before and (b) after passivation with PEDOT:PSS. The amorphous layer on the surface of the nanowire is due to the conformal coating of the polymer. TEM images of (c)  $Bi_2S_3$  nanoplatelets and (e) CdSe nanocrystals and their corresponding hybrids with PEDOT:PSS (d, f).

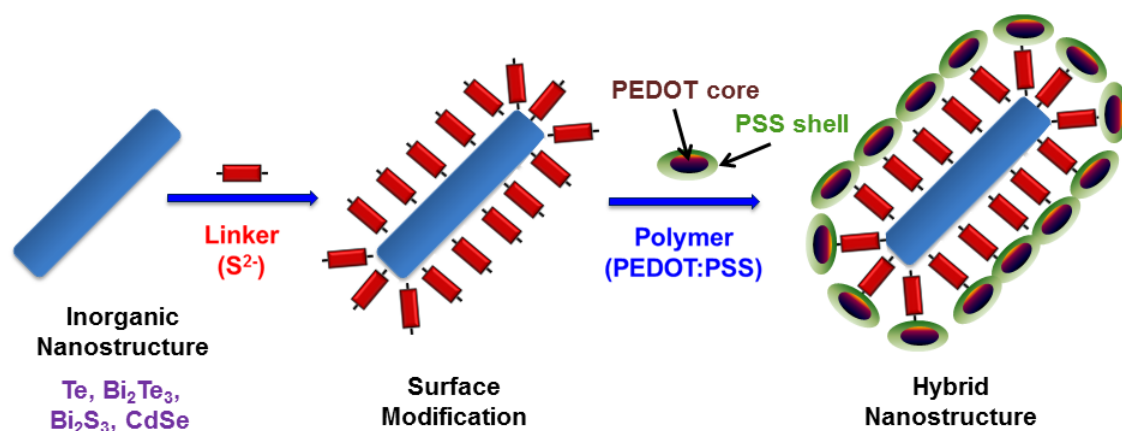
**Figure 2.** X-ray diffraction patterns for (a) tellurium nanowires and (b) bismuth sulfide nanoplatelets with as-synthesized nanostructures depicted in black, sulfur-capped nanostructures depicted in red and hybrid inorganic-PEDOT:PSS nanostructures depicted in blue. The green bars denote the reference peaks for pure bulk inorganic materials.

**Figure 3.** Dependence of (a) electrical conductivity, (b) Seebeck coefficient and (c) power factor on the weight percentage of tellurium (Te) nanowires in the hybrid film with PEDOT:PSS. The black markers represent the data from this report while the blue markers depict the data from Coates *et al.* (Ref. 35) for comparison. The red curve is a guide to the eye. Vertical error bars represent the variance of measurements over multiple samples. Horizontal error bars that represent the uncertainty in the weight percentage measurement are typically in the order of 5% and are not shown in the figure for clarity. Representative scanning electron microscopy images of hybrid Te nanowire-PEDOT:PSS films with Te nanowire weight percentages of (d) 92% (e) 82% and (f) 57%.

**Figure 4.** Dependence of (a) electrical conductivity, (b) Seebeck coefficient and (c) power factor on the weight percentage of tellurium (Te) nanowires in the hybrid film with PEDOT:PSS. The red markers represent the data from this report while the blue markers depict the data from the *in-situ* synthesis by Coates *et al.* (Ref. 35) for comparison. The red and blue curves are guides to the eye. Vertical error bars represent the variance of measurements over multiple samples. Horizontal error bars that represent the uncertainty in the weight percentage measurement are typically in the order of 5% and are not shown in the figure for clarity. Representative scanning electron microscopy images of hybrid Te nanowire-PEDOT:PSS films with Te nanowire weight percentages of (d) 94% (e) 87% and (f) 70%.

**Figure 5.** (a) Transmission electron microscope (TEM) image showing a hybrid bismuth telluride-PEDOT:PSS nanowire. The amorphous layer on the surface of the nanowire is due to the conformal coating of the polymer. (b) X-ray diffraction patterns for bismuth telluride ( $\text{Bi}_2\text{Te}_3$ ) nanowires with as-synthesized bare nanowires depicted in black, sulfur-capped nanowires depicted in red and hybrid  $\text{Bi}_2\text{Te}_3$ -PEDOT:PSS nanowires depicted in blue. The green bars denote the reference peaks for bulk  $\text{Bi}_2\text{Te}_3$ . (c) Open circuit voltage ( $V_{\text{OC}}$ ) versus applied temperature gradient ( $\Delta T$ ) for films of  $\text{Bi}_2\text{Te}_3$ -PEDOT:PSS nanowires. The Seebeck coefficient is derived from the slope of the linear fit ( $R^2$  value of 0.9998). Error bars representing the standard deviation from averaging 10 readings for each temperature gradient are captured within the data marker. (d) Raman spectra of thin films cast from pure PEDOT:PSS,  $\text{Bi}_2\text{Te}_3$ -PEDOT:PSS nanowires and PEDOT:PSS treated (reduced) with hydrazine hydrate on glass substrates. The spectra obtained from  $\text{Bi}_2\text{Te}_3$ -PEDOT:PSS nanowires matches that of reduced PEDOT:PSS indicating charge (electron) transfer from  $\text{Bi}_2\text{Te}_3$  into PEDOT:PSS.

**Figure 6.** Scheme to obtain both *p*- and *n*-type  $\text{Bi}_2\text{Te}_3$  hybrid nanostructures. Films of as-synthesized  $\text{Bi}_2\text{Te}_3$ -PEDOT:PSS nanowires are treated with formic acid to remove insulating PSS and generate high conductivity *p*-type hybrids (**a-c**) while those treated with formic acid followed by hydrazine hydrate result in *n*-type hybrids (**d-f**). Dependence of (a, d) Seebeck coefficient, (b, e) conductivity and (c, f) power factor on the weight percentage of bismuth telluride ( $\text{Bi}_2\text{Te}_3$ ) nanowires in the *p*-type and *n*-type hybrid films respectively. Horizontal error bars represent the uncertainty in the weight percentage measurement. Vertical error bars represent the variance of measurements over multiple samples. For the Seebeck measurements, the vertical error bars are captured within the data marker. The blue and red curves for the Seebeck coefficient data in (a) are from a series-connected and a parallel-connected two-component model respectively. The red curves for the data in (b-f) serve as a guide to the eye.



Scheme 1

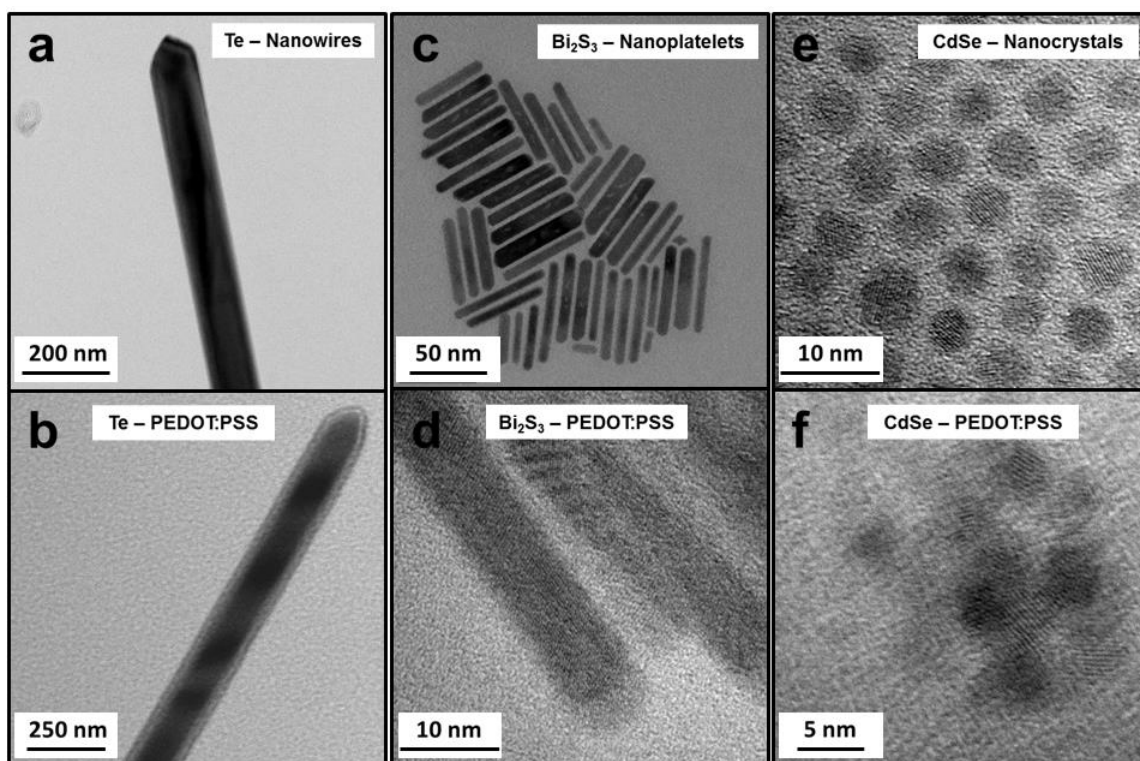


Figure 1

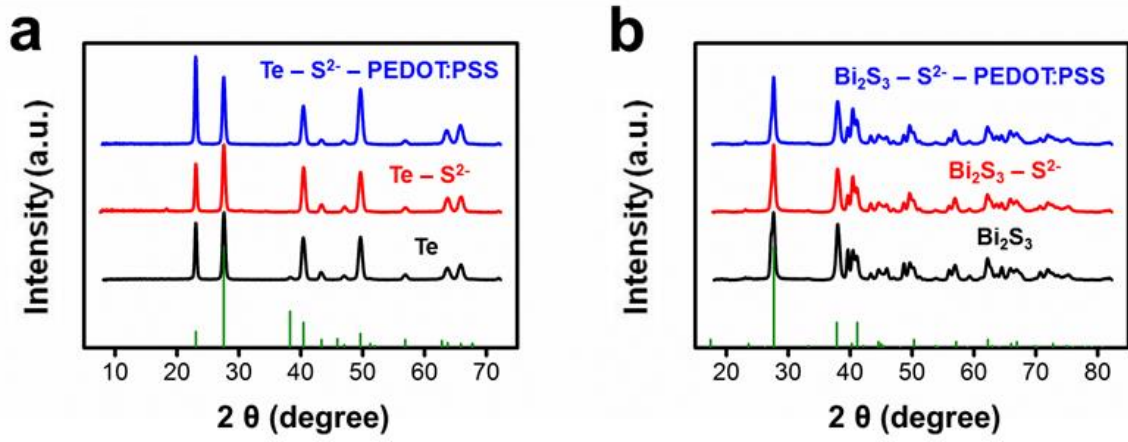


Figure 2

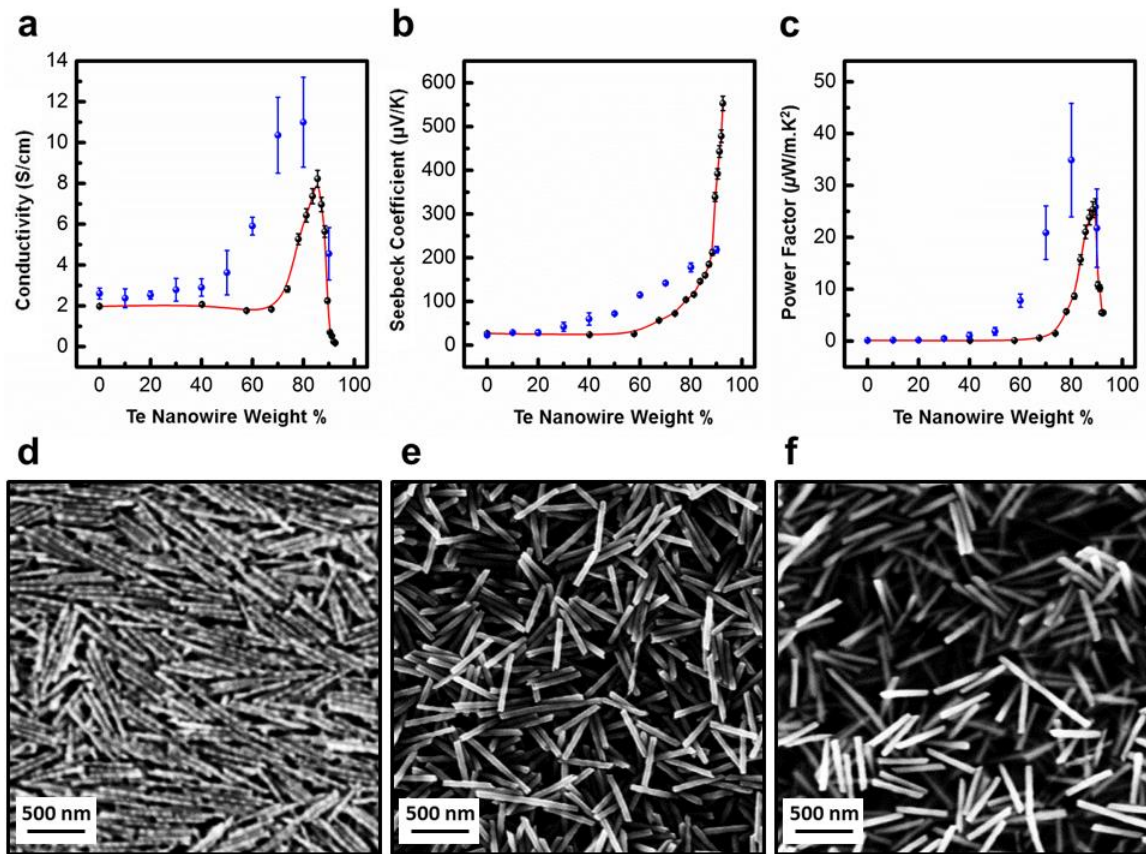


Figure 3



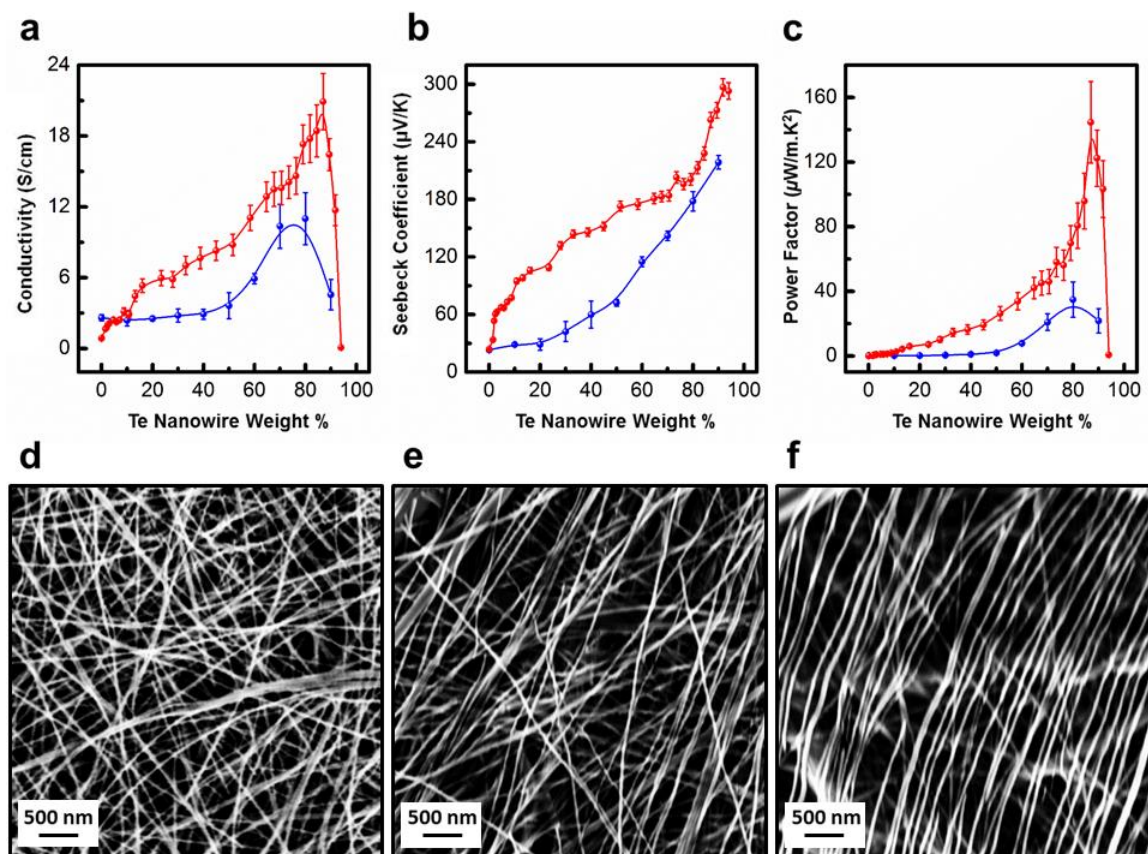


Figure 4

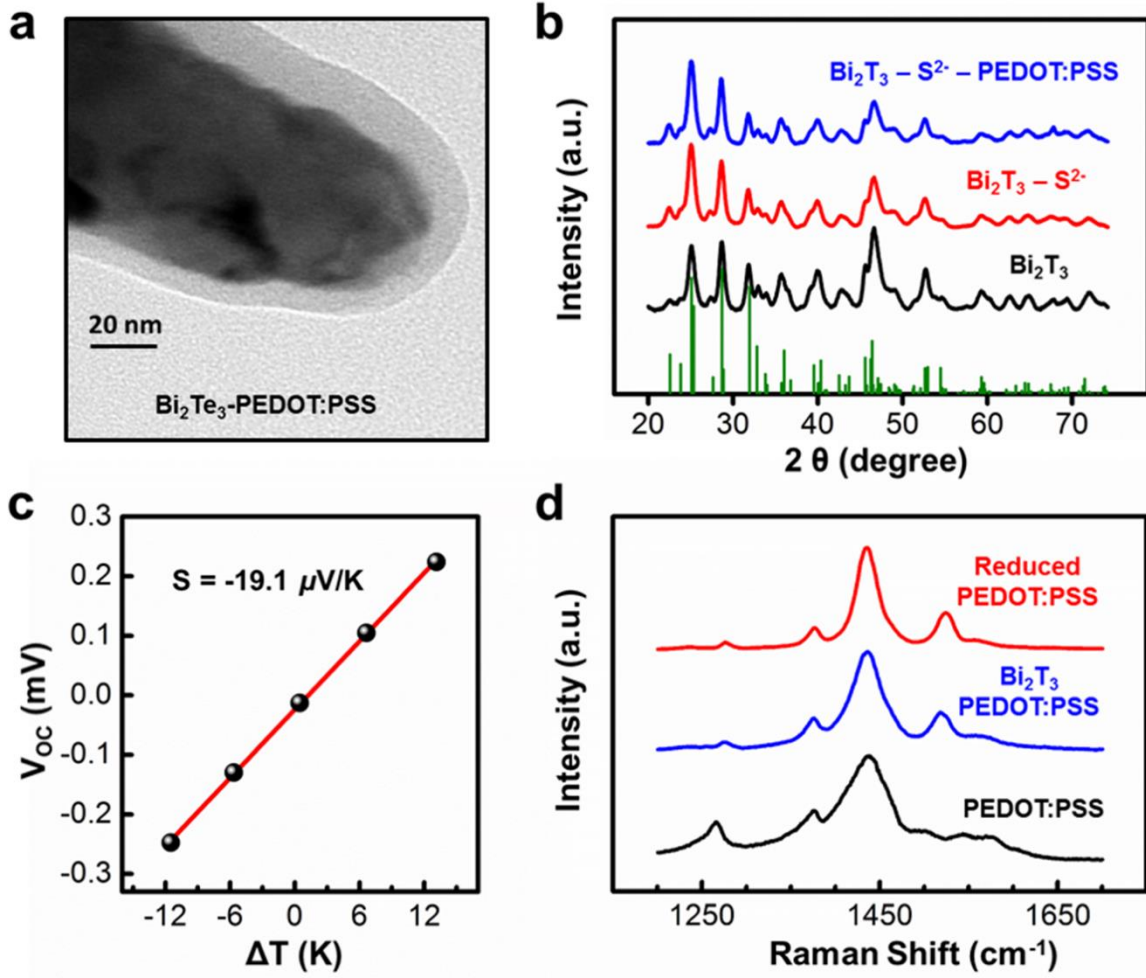


Figure 5

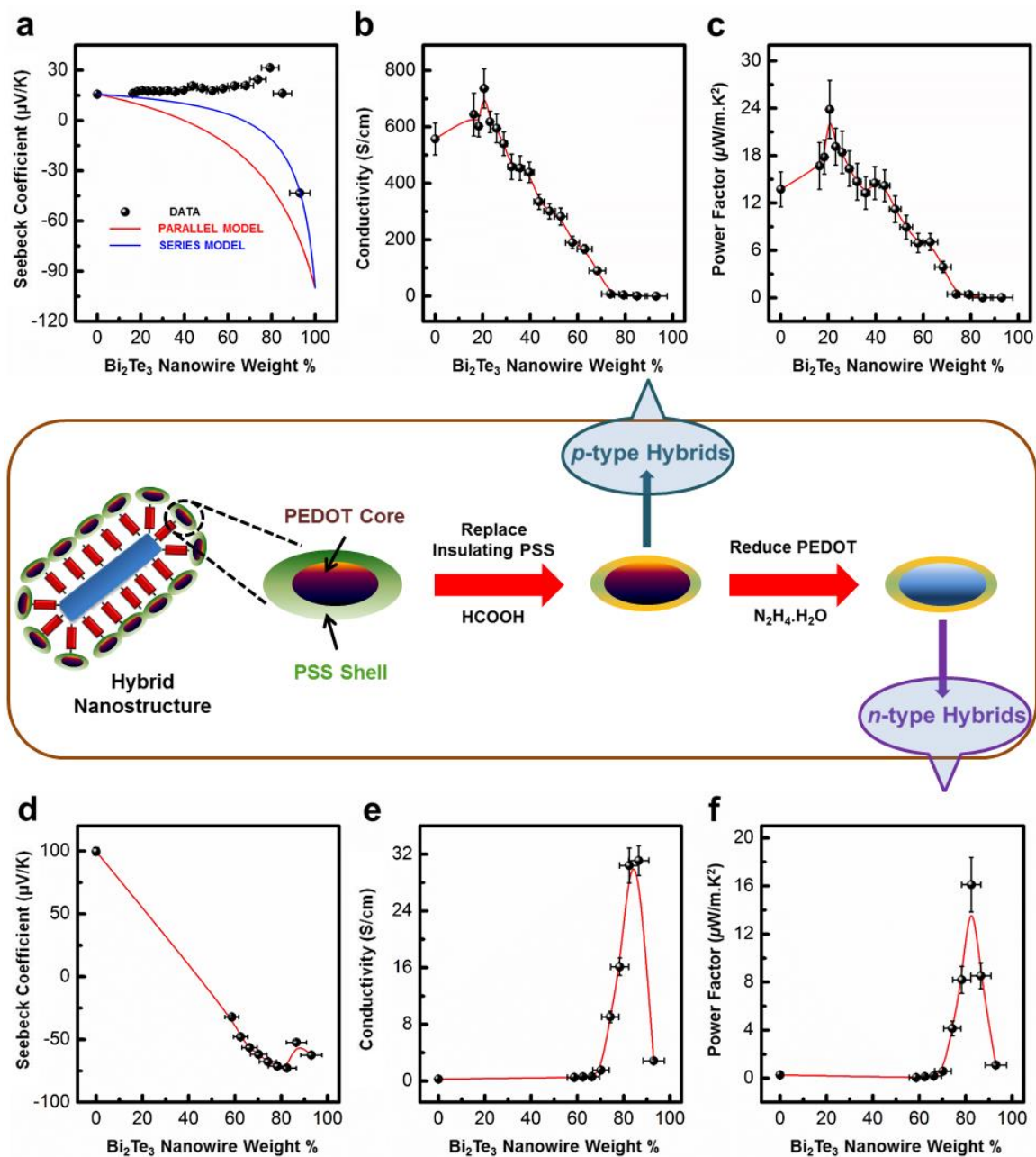


Figure 6

## References

1. L. E. Bell, *Science*, 2008, 321, 1457-1461.
2. G. J. Snyder and E. S. Toberer, *Nature Materials*, 2008, 7, 105-114.
3. T. M. Tritt and M. A. Subramanian, *MRS Bulletin*, 2006, 31, 188-194.
4. G. A. Slack and M. A. Hussain, *Journal of Applied Physics*, 1991, 70, 2694-2718.
5. G. A. Slack, in *CRC Handbook of Thermoelectrics*, CRC Press, 1995.
6. D. M. Rowe, *CRC Handbook of Thermoelectrics*, CRC Press, Boca Raton, FL, 1995.
7. D. M. Rowe, *Journal of Physics F-Metal Physics*, 1974, 7, 1843-1846.
8. G. D. Mahan and J. O. Sofo, *Proceedings of the National Academy of Sciences of the United States of America*, 1996, 93, 7436-7439.
9. L. D. Hicks and M. S. Dresselhaus, *Physical Review B*, 1993, 47, 16631-16634.
10. R. Venkatasubramanian, E. Siivola, T. Colpitts and B. O'Quinn, *Nature*, 2001, 413, 597-602.
11. T. C. Harman, P. J. Taylor, M. P. Walsh and B. E. LaForge, *Science*, 2002, 297, 2229-2232.
12. A. I. Hochbaum, R. Chen, R. D. Delgado, W. Liang, E. C. Garnett, M. Najarian, A. Majumdar and P. Yang, *Nature*, 2008, 451, 163-167.
13. B. Poudel, Q. Hao, Y. Ma, Y. Lan, A. Minnich, B. Yu, X. Yan, D. Wang, A. Muto, D. Vashaee, X. Chen, J. Liu, M. S. Dresselhaus, G. Chen and Z. Ren, *Science*, 2008, 320, 634-638.
14. J. P. Heremans, V. Jovovic, E. S. Toberer, A. Saramat, K. Kurosaki, A. Charoenphakdee, S. Yamanaka and G. J. Snyder, *Science*, 2008, 321, 554-557.
15. A. I. Boukai, Y. Bunimovich, J. Tahir-Kheli, J.-K. Yu, W. A. Goddard, III and J. R. Heath, *Nature*, 2008, 451, 168-171.
16. W. Kim, J. Zide, A. Gossard, D. Klenov, S. Stemmer, A. Shakouri and A. Majumdar, *Physical Review Letters*, 2006, 96, 045901.
17. C. J. Vineis, A. Shakouri, A. Majumdar and M. G. Kanatzidis, *Advanced Materials*, 2010, 22, 3970-3980.
18. M. S. Dresselhaus, G. Chen, M. Y. Tang, R. G. Yang, H. Lee, D. Z. Wang, Z. F. Ren, J. P. Fleurial and P. Gogna, *Advanced Materials*, 2007, 19, 1043-1053.
19. Z. Han and A. Fina, *Progress in Polymer Science*, 2011, 36, 914-944.
20. K. Harada, M. Sumino, C. Adachi, S. Tanaka and K. Miyazaki, *Applied Physics Letters*, 2010, 96, 253304.
21. O. Bubnova, Z. U. Khan, A. Malti, S. Braun, M. Fahlman, M. Berggren and X. Crispin, *Nature Materials*, 2011, 10, 429-433.
22. G. H. Kim, L. Shao, K. Zhang and K. P. Pipe, *Nature Materials*, 2013, 12, 719-723.

23. C.-K. Mai, B. Russ, S. L. Fronk, N. Hu, M. B. Chan-Park, J. J. Urban, R. A. Segalman, M. L. Chabinyk and G. C. Bazan, *Energy & Environmental Science*, 2015, 8, 2341-2346.
24. B. Russ, M. J. Robb, F. G. Brunetti, P. L. Miller, E. E. Perry, S. N. Patel, V. Ho, W. B. Chang, J. J. Urban, M. L. Chabinyk, C. J. Hawker and R. A. Segalman, *Advanced Materials*, 2014, 26, 3473-3477.
25. E. S. Cho, N. E. Coates, J. D. Forster, A. M. Ruminski, B. Russ, A. Sahu, N. C. Su, F. Yang and J. J. Urban, *Advanced Materials*, 2015, 27, 5744-5752.
26. A. Facchetti, *Chemistry of Materials*, 2011, 23, 733-758.
27. D. V. Talapin, J.-S. Lee, M. V. Kovalenko and E. V. Shevchenko, *Chemical Reviews*, 2010, 110, 389-458.
28. C. Sanchez, P. Belleville, M. Popall and L. Nicole, *Chem. Soc. Rev.*, 2011, 40, 696-753.
29. H. C. Kolb, M. G. Finn and K. B. Sharpless, *Angewandte Chemie International Edition*, 2001, 40, 2004-2021.
30. B. Zhang, J. Sun, H. E. Katz, F. Fang and R. L. Opila, *ACS Applied Materials & Interfaces*, 2010, 2, 3170-3178.
31. K. C. See, J. P. Feser, C. E. Chen, A. Majumdar, J. J. Urban and R. A. Segalman, *Nano Letters*, 2010, 10, 4664-4667.
32. M. He, J. Ge, Z. Lin, X. Feng, X. Wang, H. Lu, Y. Yang and F. Qiu, *Energy & Environmental Science*, 2012, 5, 8351-8358.
33. N. E. Coates, S. K. Yee, B. McCulloch, K. C. See, A. Majumdar, R. A. Segalman and J. J. Urban, *Advanced Materials*, 2013, 25, 1629-1633.
34. S. K. Yee, N. E. Coates, A. Majumdar, J. J. Urban and R. A. Segalman, *Physical Chemistry Chemical Physics*, 2013, 15, 4024-4032.
35. Y. Du, K. F. Cai, S. Chen, P. Cizek and T. Lin, *ACS Applied Materials & Interfaces*, 2014, 6, 5735-5743.
36. J. N. Heyman, B. A. Alebachew, Z. S. Kaminski, M. D. Nguyen, N. E. Coates and J. J. Urban, *Applied Physics Letters*, 2014, 104, 141912.
37. J. N. Heyman, A. Sahu, N. E. Coates, B. Ehmman and J. J. Urban, *MRS Online Proceedings Library*, 2015, 1742.
38. B. R. Saunders and M. L. Turner, *Advances in Colloid and Interface Science*, 2008, 138, 1-23.
39. E. Holder, N. Tessler and A. L. Rogach, *Journal of Materials Chemistry*, 2008, 18, 1064-1078.
40. B. Mayers, B. Gates, Y. Yin and Y. Xia, *Advanced Materials*, 2001, 13, 1380-1384.
41. G. Q. Zhang, H. Y. Fang, H. R. Yang, L. A. Jauregui, Y. P. Chen and Y. Wu, *Nano Letters*, 2012, 12, 3627-3633.
42. G. Q. Zhang, B. Kirk, L. A. Jauregui, H. R. Yang, X. F. Xu, Y. P. Chen and Y. Wu, *Nano Letters*, 2011, 12, 56-60.
43. S. H. Lee, H. Park, S. Kim, W. Son, I. W. Cheong and J. H. Kim, *Journal of Materials Chemistry A*, 2014, 2, 7288-7294.
44. J. Ouyang, Q. Xu, C.-W. Chu, Y. Yang, G. Li and J. Shinar, *Polymer*, 2004, 45, 8443-8450.

45. S. Garreau, G. Louarn, J. P. Buisson, G. Froyer and S. Lefrant, *Macromolecules*, 1999, 32, 6807-6812.
46. W. W. Chiu, J. Travas-Sejdic, R. P. Cooney and G. A. Bowmaker, *Synth. Met.*, 2005, 155, 80-88.
47. W. W. Chiu, J. Travas-Sejdic, R. P. Cooney and G. A. Bowmaker, *J. Raman Spectrosc.*, 2006, 37, 1354-1361.
48. N. Massonnet, A. Carella, O. Jaudouin, P. Rannou, G. Laval, C. Celle and J.-P. Simonato, *Journal of Materials Chemistry C*, 2014, 2, 1278-1283.
49. I. Cruz-Cruz, M. Reyes-Reyes, I. A. Rosales-Gallegos, A. Y. Gorbachev, J. M. Flores-Camacho and R. López-Sandoval, *The Journal of Physical Chemistry C*, 2015, 119, 19305-19311.
50. Y. Gelbstein, *Journal of Applied Physics*, 2009, 105, 023713.
51. D. A. Mengistie, M. A. Ibrahim, P.-C. Wang and C.-W. Chu, *ACS Applied Materials & Interfaces*, 2014, 6, 2292-2299.
52. P. Reiss, J. Bleuse and A. Pron, *Nano Letters*, 2002, 2, 781-784.
53. R. Malakooti, L. Cademartiri, Y. Akcakir, S. Petrov, A. Migliori and G. A. Ozin, *Advanced Materials*, 2006, 18, 2189-2194.